The role of effectiveness factor on the modeling of methanol steam reforming over CuO/ZnO/Al2O3 catalyst in a multi-tubular reactor

Zhu, Jimin; Simon Araya, Samuel; Cui, Xiaoti; Kær, Søren Knudsen

Published in:
International Journal of Hydrogen Energy

DOI (link to publication from Publisher):
10.1016/j.ijhydene.2021.12.223

Publication date:
2022

Document Version
Publisher's PDF, also known as Version of record

Available online at www.sciencedirect.com

ScienceDirect

journal homepage: www.elsevier.com/locate/he

The role of effectiveness factor on the modeling of methanol steam reforming over CuO/ZnO/Al_2O_3 catalyst in a multi-tubular reactor

Jimin Zhu[*], *Samuel Simon Araya*, *Xiaoti Cui*, *Søren Knudsen Kær*

AAU Energy, Aalborg University, Pontoppidanstraede 111, 9220, Aalborg øst, Denmark

HIGHLIGHTS

- One-dimensional pseudo-homogeneous model of a packed-bed methanol steam reformer.
- Two methods to obtain approximate solutions of the catalytic effectiveness factor.
- Validation of reaction kinetics and effectiveness factors with experimental data.
- Effects of main operating parameters on the intraparticle heat and mass transfer.
- Optimized conditions to obtain less than 1% of CH_3OH and CO in reformate gas.

GRAPHICAL ABSTRACT

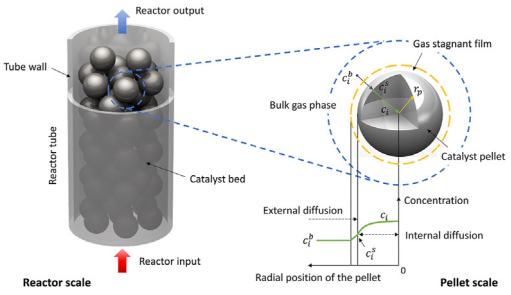

ARTICLE INFO

Article history:
Received 19 August 2021
Received in revised form
23 December 2021
Accepted 24 December 2021
Available online xxx

Keywords:
Methanol steam reforming
Intraparticle diffusion
Thiele modulus

ABSTRACT

A pseudo-homogeneous model for the methanol steam reforming process was developed based on reaction kinetics over a CuO/ZnO/Al_2O_3 catalyst and non-adiabatic heat and mass transfer performances in a co-current packed-bed reactor. A Thiele modulus method and an intraparticle distribution method were applied for predicting the effectiveness factors for main reactions and providing insights into the diffusion-reaction process in a cylindrical catalyst pellet. The results of both methods are validated and show good agreements with the experimental data, but the intraparticle distribution method provides better predictions. Results indicate that increases in catalyst size and bulk fluid temperature amplify the impact of intraparticle diffusion limitations, showing a decrease in effectiveness factors. To satisfy the requirements of a high temperature polymer electrolyte membrane fuel cell stack, the optimized operating conditions, which

* *Corresponding author.*
E-mail address: jzu@energy.aau.dk (J. Zhu).

https://doi.org/10.1016/j.ijhydene.2021.12.223

Effectiveness factor
Hydrogen production

bring the methanol and CO concentrations to less than 1% vol in the reformate stream, are determined based on the simulation results.

Introduction

Hydrogen is a clean and promising energy carrier and plays an essential role in hydrogen-based energy systems, especially in polymer electrolyte membrane (PEM) fuel cell systems. Among PEM fuel cells, high-temperature polymer electrolyte membrane (HT-PEM) fuel cells show advantages in enhanced electrode kinetics and easier heat and water management [1,2]. By operating at a higher temperature (393 – 473 K), HT-PEM fuel cells also have an improved tolerance towards carbon monoxide (CO) up to 3 – 5% vol [3–5].

Hydrogen, however, has a low volumetric density and shows limitations in terms of storage, transportation, and distribution, which are existing barriers to the growth of the hydrogen market [6,7]. Reforming of carbon-based fuels such as natural gas, methane and methanol is a promising technology for hydrogen production [8]. Among all these fuels, methanol is a good hydrogen source because it is in liquid form under standard conditions and has a high hydrogen to carbon ratio (4 : 1). Methanol has both a high gravimetric energy density (22.4 MJ kg^{-1} vs. less than 1 MJ kg^{-1} for batteries or pumped hydro storage) and a high volumetric energy density (17.8 MJ L^{-1} vs. 0.01 MJ L^{-1} and 0.03 MJ L^{-1} for hydrogen and methane, respectively) [9]. The high energy density and stability of methanol at ambient conditions make it cheap and easy for long-term storage. A lower reforming temperature (473 – 573 K) than other carbon-based fuels such as methane (1073 – 1273 K) also makes it suitable for stack integration with HT-PEM fuel cells [4,8]. Moreover, methanol can be produced from renewable energies and captured carbon dioxide (CO_2), which benefits from the extensive studies of power-to-methanol technology. Therefore, it can be considered as a decarbonized energy carrier [9,10]. The most commonly used reforming method for methanol is catalytic steam reforming. Compared with other methanol-reforming methods, the methanol steam reforming (MSR) process provides the highest concentration of hydrogen per mole of methanol [11,12]. The following three reactions are considered to represent the kinetics of the MSR process [13,14]:

Methanol steam reforming reaction (MSR)

$$CH_3OH + H_2O \leftrightarrow CO_2 + 3H_2 \quad \Delta H = +49.7\ (\text{kJ mol}^{-1}) \tag{1}$$

Water-gas shift reaction (WGS)

$$CO + H_2O \leftrightarrow CO_2 + H_2 \quad \Delta H = -41.2\ (\text{kJ mol}^{-1}) \tag{2}$$

Methanol decomposition reaction (MD)

$$CH_3OH \leftrightarrow CO + 2H_2 \quad \Delta H = +90.2\ (\text{kJ mol}^{-1}) \tag{3}$$

The most commonly used catalysts for MSR process are copper-based catalysts, especially $CuO/ZnO/Al_2O_3$ catalysts, because of their high activity and selectivity [8,15,16]. Inside a porous catalyst pellet, chemical reactions and heat and mass transfer take place simultaneously. Typically, experiments reported in the literature were conducted on finely powdered catalysts [8,17]. Hence, the intraparticle diffusion resistances can be ignored and the reaction rates are referred to as intrinsic. In industrial-scale applications, however, it is not possible to use such tiny catalyst pellets without causing significant pressure drops [18].

Diffusion limitations inside catalyst pellets can affect the local reaction rates and selectivity, especially for larger particle sizes and at higher operating temperatures [19]. To accurately predict the reforming performance of the catalyst bed, the effectiveness factor (η) should be introduced. The effectiveness factor is used to quantify the effect of intraparticle diffusion limitations on reaction rates. It is defined as the ratio of the actual reaction rate in the catalyst particle to the calculated rate that exists in the absence of diffusion limitations [20–23].

One of the most commonly used methods to calculate the effectiveness factor is using the Thiele modulus by assuming an isothermal, first-order reaction [21,24–26]. The Thiele modulus is a non-dimensional number representing the relationship between the diffusion rate and the reaction rate in a porous catalyst pellet. Another way to estimate the effectiveness factor is by considering the temperature and concentration distributions inside the catalyst particle, known as intraparticle distribution method. In this method, the equations of reaction rates and mass and energy balances are numerically solved to obtain the temperature and concentration distributions and the local reaction rates within the catalyst particle [27–30].

$$\eta = \frac{\text{Actual overall rate of reaction}}{\text{Rate of reaction that would result if entire interior surface were exposed to the external pellet surface conditions } C_{is}, T_s} \tag{4}$$

Please cite this article as: Zhu J et al., The role of effectiveness factor on the modeling of methanol steam reforming over $CuO/ZnO/Al_2O_3$ catalyst in a multi-tubular reactor, International Journal of Hydrogen Energy, https://doi.org/10.1016/j.ijhydene.2021.12.223

Hafeez et al. [26] developed a heterogeneous model to predict the performance of both a packed bed and a coated wall microreactor over a commercial $CuO/ZnO/Al_2O_3$ catalyst. In their study, the effectiveness factor was calculated using the Thiele modulus. The MSR and MD reactions were considered irreversible, and the WGS reaction was neglected. Ziarati et al. [28] developed a dynamic model of the MSR process in a packed-bed reactor considering the contributions of all molecular and convective terms of momentum, heat and mass transfer, and the effectiveness factors. They used the species continuity equations to calculate the intraparticle concentration distributions of methanol, hence to estimate the effectiveness factor for the MSR reaction. However, the WGS reaction was neglected. The effectiveness factor for the MD reaction was also considered as equal to one. Olatunde et al. [29] numerically investigated the non-isothermal effectiveness factor for the catalytic MSR process over a commercial $CuO/ZnO/Al_2O_3$ catalyst. The concentration distribution of key components (methanol and hydrogen) and the temperature distribution inside a spherical catalyst pellet was estimated. However, they neglected the external diffusion resistances between gas and solid phase. The existence of CO was also neglected in the reforming mixture. Tesser et al. [30] conducted the experimental work on an internal loop gradient-less Berty CSTR reactor and a pilot-scale tubular packed-bed reactor for MSR. A reactor model taking into account the reaction kinetics and mass and heat transfer effects was also developed. The effectiveness factor was considered for a commercial catalyst in the size of 3–7 mm. The effectiveness factor was calculated by solving mass and heat balance equations governing the simultaneous reactions and diffusion in a catalyst particle. However, the reaction mechanisms for CO formation were not considered in their study. Indeed, most studies regard the MSR process as a first-order reaction when calculating the effectiveness factor. Some studies ignore the external mass transfer limitations. Moreover, some researches do not appropriately deal with complex reaction networks inside the catalyst particle [25].

In our previous work [31], a one-dimensional pseudo-homogeneous model for the MSR process in a packed bed reactor was proposed. The effectiveness factor for the MSR reaction was calculated by using an empirical equation of the Thiele modulus. However, the effectiveness factors for the WGS and MD reactions were ignored. Moreover, the role of the intraparticle diffusion resistances as well as the effectiveness factors on the performance of the reactor are not well investigated, adding to the novelty of this work.

In the current study, a one-dimensional steady-state model of a multi-tubular packed-bed reformer was developed for the steam reforming of methanol on a commercial $CuO/ZnO/Al_2O_3$ catalyst. A comprehensive kinetic Langmuir-Hinshelwood model was proposed to express the rate of MSR, WGS and MD reactions. The effectiveness factor for the MSR reaction was calculated as a function of the Thiele modulus, which could be seen from our previous work [31]. For comparison purposes, a rigorous reaction-diffusion model in catalyst pellets was also developed to estimate the effectiveness factors. The effects of key operating parameters (temperature and particle size) on the intraparticle distributions of temperature and concentration were studied and discussed. As opposed to previous pseudo-homogeneous models, this model provided an understanding of the role of the external and internal heat and mass transfer resistances in effectiveness factors, and appropriately dealt with the transport phenomena and complex reaction networks inside catalyst particles. In addition, experiments were conducted in this study to validate the kinetic model and the effectiveness factors. To bring both the methanol and CO concentrations to less than 1% vol in the reformate stream, the optimized operating conditions were determined based on the simulation results.

Design of methanol steam reformer

Generally, a reformed methanol fuel cell (RMFC) system is composed of a burner, an evaporator, several thermal fluid circuits, a methanol steam reformer, and a high temperature PEM fuel cell stack. During the operation, a mixture of methanol and water is pumped into the evaporator, where the fuel is evaporated and then fed into the catalyst bed in the reformer. The reactants in the bulk fluid first travel to the external surface of the catalyst pellets, then diffuse from the external surface into and through the pores within the pellets, where the reactions take place on the exposed surface of catalyst. After that, the produced hydrogen-rich gas is sent to the anode side of the fuel cell stack. The fuel cells utilize the hydrogen from the anode side together with the oxygen from the cathode side to generate electricity by electrochemical reactions. The exhaust gas from the fuel cell stack anode is directed to the burner, where the residual carbon monoxide, hydrogen, and methanol react with air to generate thermal energy through the combustion process. The generated heat is provided into the catalyst bed by the thermal fluid passing through the shell side of the reactor. In this work, the methanol steam reformer as a subsystem of the RMFC system has been studied.

The shell-and-tube reformer for MSR in this study consists of baffles and tubes inside a cylindrical shell. The structure of the multi-tubular packed-bed reactor is illustrated in Fig. 1. The reactor shell is usually surrounded by thermal insulation materials to avoid any significant amount of heat loss. Tubes packed with $CuO/ZnO/Al_2O_3$ catalyst are installed inside the shell and arranged in equilateral triangle tube bundles. The baffle plates are used to support the tube bundles, increase the flow distribution in the inter-tubular space, and for an effective heat transfer between tube and shell sides. The gas from the burner flows through the shell side of the reformer, thereby providing an external heat source to drive the reactions in the catalyst bed. In the tube side, reactants flow through the catalyst bed, where the steam reforming reactions and pressure drop occur.

Please cite this article as: Zhu J et al., The role of effectiveness factor on the modeling of methanol steam reforming over $CuO/ZnO/Al_2O_3$ catalyst in a multi-tubular reactor, International Journal of Hydrogen Energy, https://doi.org/10.1016/j.ijhydene.2021.12.223

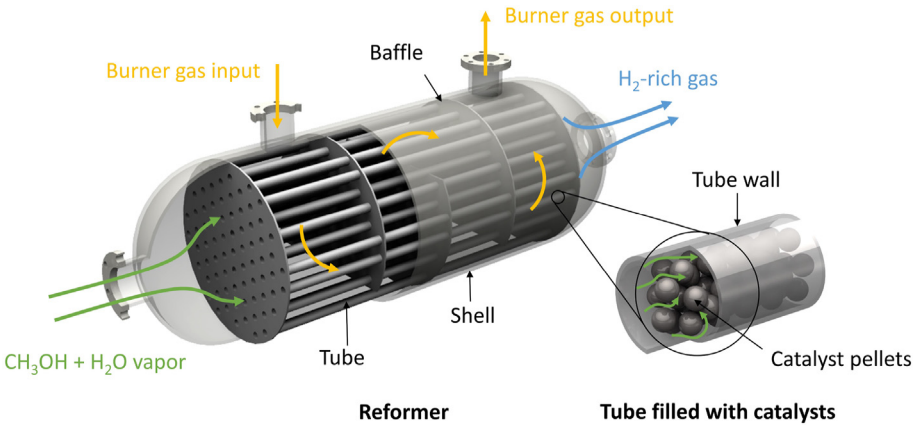

Fig. 1 – Schematic diagram of a multi-tubular packed-bed reactor for methanol steam reforming.

Experiment

Experimental setup

Experiments for the MSR process were performed at atmospheric pressure in a small-scale packed-bed reactor made of stainless steel. The commercial $CuO/ZnO/Al_2O_3$ catalyst particles were loaded in the reactor. The feeding rate of fuel (liquid methanol-water mixture) from the fuel tank was measured and controlled by a mass flow controller (MFC). The methanol-water mixture was first pumped into the evaporator, where the mixture was heated and evaporated. The high-temperature steam and methanol vapor then passed through the catalyst bed, where a fine mesh grid supported the catalysts. The reactor was surrounded by thermal insulation materials and heated by electric heaters outside the reactor. Therefore, this packed-bed reactor is assumed to be isothermal. The electric heaters were regulated by PID control of the electric heaters to maintain the temperature in the fixed bed within a specific range. Temperatures at the inlet and outlet of the reactor were measured by two thermocouples. The average value of the measured inlet and outlet temperatures was regarded as the temperature of the catalyst bed. The gas analyzer (SIEMENS FIDMAT 6 for CH_3OH, CALOMAT 6 for H_2, and ULTRAMAT 6 for CO and CO_2) was used to analyze the main components of the reformate stream from the MSR reactor. The basic schematic of the experimental setup is shown in Fig. 2.

Experimental procedure

The reactor was loaded with 3.66 g of the commercial $CuO/ZnO/Al_2O_3$ catalyst in a volume of 3.6 mL. Cylindrical catalyst particles with a diameter of 1.5 mm were used. The catalyst was flushed firstly in situ with a volumetric flow rate of hydrogen $Q_{H_2} = 0.1\ cm^3\ min^{-1}$, and a volumetric flow rate of dinitrogen $Q_{N_2} = 2\ cm^3\ min^{-1}$ (5% vol of H_2 diluted with N_2) for 1 h to reduce CuO to Cu (the main active component in the catalyst). The reduction reaction rate was kept low in order to avoid any sintering of catalyst by controlling the operating temperature in the range of 433–493 K. The reforming process was carried out at temperatures of 493 K, 513 K and 533 K and a ratio of catalyst weight to the molar flow rate of

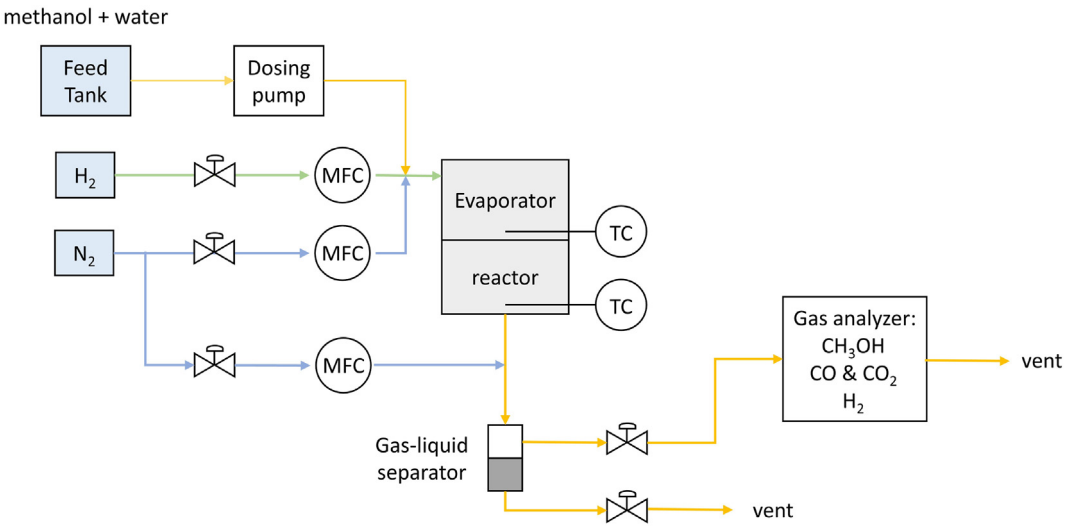

Fig. 2 – Processflow-sheet for the experimental setup.

Please cite this article as: Zhu J et al., The role of effectiveness factor on the modeling of methanol steam reforming over $CuO/ZnO/Al_2O_3$ catalyst in a multi-tubular reactor, International Journal of Hydrogen Energy, https://doi.org/10.1016/j.ijhydene.2021.12.223

methanol (W/F_{CH_3OH}) in the range of 44 – 263 kg s mol^{-1}. The variation of W/F_{CH_3OH} was achieved by changing the volumetric flow rate of liquid methanol Q_{CH_3OH} from 0.051 to 0.308 cm^3 min^{-1} while keeping a constant catalyst loading. Test at each operating condition was kept for at least 30 min of continuous running to make sure the steady state was achieved. The value of the steam to carbon ration (S/C) was selected to be 1.3 to maximize the methanol conversion without wasting much energy in water evaporation [32].

Mathematical model

The phenomena occurring in the catalytic packed-bed reactor for MSR can be characterized according to the reaction kinetics, pressure drop, internal and external diffusion resistances of catalyst pellets, heat and mass transfer in both tube and shell sides, and heat exchange between the tube side and shell side through the tube wall. Therefore, the one-dimensional pseudo-homogeneous model is developed taking into account the reaction kinetics, effectiveness factors, species continuity equation, thermal energy equation, and pressure drop.

Reaction kinetics

According to the studies of Sá et al. [33] and Herdem et al. [34], the kinetic Langmuir-Hinshelwood model based on the work of Peppley et al. [13,14] has been proved to present the best agreement between the mathematical model and the experimental data for the commercial $CuO/ZnO/Al_2O_3$ catalyst. Peppley et al. [13,14] developed a comprehensive model for the process of MSR on a $CuO/ZnO/Al_2O_3$ catalyst. The surface mechanisms for all three reversible reactions (MSR, WGS, and MD) were proposed based on the following assumptions: hydrogen adsorption doesn't compete for the same active sites with the adsorption of oxygen-containing species; the type of active sites for the MD reaction is different from the type of active sites for the MSR and WGS reactions; the rate-determining step for both the MSR reaction and MD reaction is the dehydrogenating of adsorbed methoxy groups; the rate-determining step for the WGS reaction is the formation of an intermediate formate species. The detailed derivations of the rate expressions are reported in Ref. [35]. Based on the Langmuir-Hinshelwood model, the rate expressions for the three main reactions (MSR, WGS and MD) involved in the process can be expressed as:

$$r_R = \frac{k_R K^*_{CH_3O^{(1)}} \left(p_{CH_3O\ H} \Big/ p^{1/2}_{H_2}\right)\left(1 - p^3_{H_2} p_{Co_2} \Big/ K^{eq}_R p_{CH_3\ OH}\, p_{H_2o}\right) C^T_{S_1} C^T_{S_{1a}}}{\left(1 + K^*_{CH_3O^{(1)}} \left(p_{CH_3O\ H} \Big/ p^{1/2}_{H_2}\right) + K^*_{HCO\ O^{(1)}} p_{CO_2} p^{1/2}_{H_2} + K^*_{OH^{(1)}} \left(p_{H_2O} \Big/ p^{1/2}_{H_2}\right)\right)\left(1 + K^{1/2}_{H^{(1a)}} p^{1/2}_{H_2}\right)} \tag{5}$$

$$r_W = \frac{k_W K^*_{OH^{(1)}} \left(p_{CO} p_{H_2O} \Big/ p^{1/2}_{H_2}\right)\left(1 - p_{H_2} p_{CO_2} \Big/ K^{eq}_W p_{CO} p_{H_2o}\right) C^{T^2}_{S_1}}{\left(1 + K^*_{CH_3O^{(1)}} \left(p_{CH_3O\ H} \Big/ p^{1/2}_{H_2}\right) + K^*_{HCO\ O^{(1)}} p_{CO_2} p^{1/2}_{H_2} + K^*_{OH^{(1)}} \left(p_{H_2o} \Big/ p^{1/2}_{H_2}\right)\right)^2} \tag{6}$$

$$r_D = \frac{k_D K^*_{CH_3O^{(2)}} \left(p_{CH_3O\ H} \Big/ p^{1/2}_{H_2}\right)\left(1 - p^2_{H_2} p_{CO} \Big/ K^{eq}_D p_{CH_3O\ H}\right) C^T_{S_2} C^T_{S_{2a}}}{\left(1 + K^*_{CH_3O^{(2)}} \left(p_{CH_3O\ H} \Big/ p^{1/2}_{H_2}\right) + K^*_{OH^{(2)}} \left(p_{H_2O} \Big/ p^{1/2}_{H_2}\right)\right)\left(1 + K^{1/2}_{H^{(2a)}} p^{1/2}_{H_2}\right)} \tag{7}$$

where r_j (mol m^{-2} s^{-1}) is the rate of reaction j (j = R, W and D); k_j and K^{eq}_j (m^2 s^{-1} mol^{-1}) are the equilibrium constant of reaction j, respectively; and K^* (bar$^{-0.5}$) is the adsorption coefficient; p_i (bar) is the partial pressure of component i ($i = CO_2, CO, H_2, CH_3OH$ and H_2O). Based on the reaction mechanisms, the elementary surface processes for the MSR and the WGS reactions occur on the Type 1 active sites, and the MD reaction occurs on the distinct Type 2 active site. Therefore, the $C^T_{s_1}$, $C^T_{s_{1a}}$, $C^T_{s_2}$ and $C^T_{s_{2a}}$ in equations (5)–(7) are defined as the concentrations of distinct active sites '1′, '1a′, '2′, and '2a' on the surface of the catalyst (mol m^{-2}), where the '1′ and '1a' sites are assumed to be active for the MSR and WGS reactions and the '2′ and '2a′ sites are for the MD reaction [14].

Effectiveness factor

When there are considerable heat and mass transfer resistances inside the porous catalyst particle, the reaction rates on the catalyst particle can be non-uniform. To account for variations in the reaction rates throughout the pellet, a parameter known as the effectiveness factor is introduced. The effectiveness factor η is defined as the ratio of the actual reaction rate in the catalyst particle to the reaction rate at the external surface of the pellet [21]. It can be obtained as a function of the Thiele modulus for first-order kinetics in a spherical catalyst pellet. Another approach is to calculate the effectiveness factor numerically by considering the concentration and temperature distributions within catalyst pellets.

Thiele modulus method

A Thiele modulus-effectiveness factor method is applied to provide insight into the interplay of intraparticle mass transfer and intrinsic adsorption kinetics [36]. For a first-order reaction in spherical catalyst pellets, the expression of the effectiveness factor as a function of Thiele modulus is:

$$\eta = \frac{3}{\varphi_1^2}(\varphi_1 \coth \varphi_1 - 1) \tag{8}$$

where φ_1 is the Thiele modulus for a first-order reaction, which can be expressed as:

Please cite this article as: Zhu J et al., The role of effectiveness factor on the modeling of methanol steam reforming over $CuO/ZnO/Al_2O_3$ catalyst in a multi-tubular reactor, International Journal of Hydrogen Energy, https://doi.org/10.1016/j.ijhydene.2021.12.223

$$\varphi_1^2 = \frac{r_{js}\rho_c r_p^2 S_c}{D_{i,ep} c_{is}} \quad (9)$$

where r_{js} (mol m^{-2} s^{-1}) and c_{is} (mol m^{-3}) are the rate of reaction j and the concentration of component i if the entire interior surface was exposed; r_p (m) is the radius of the catalyst pellet; ρ_c (kg m^{-3}) is the density of catalyst bed; and $D_{i,ep}$ (m^2 s^{-1}) is the effective diffusivity of component i, which is defined to describe the diffusion that affects the chemical reactions inside catalyst particles.

The catalyst particle used in this study is cylindrical with an aspect ratio of 1. For such a non-spherical particle, the volume-equivalent (surface-equivalent) particle diameter, defined as the diameter of a single spherical pellet having the same volume (surface) as the non-spherical particle, is introduced in this study. For a cylinder catalyst with a diameter d and a height h, the volume-equivalent particle diameter d_p^v can be calculated by:

$$d_p^v = \left(\frac{6V_{pa}}{\pi}\right)^{\frac{1}{3}} = d\left(\frac{3}{2}\frac{h}{d}\right)^{\frac{1}{3}} \quad (10)$$

where V_{pa} (m^3) is the volume of a single catalyst particle. The surface-equivalent sphere diameter d_p^s (m) can be calculated by:

$$d_p^s = \left(\frac{S_{pa}}{\pi}\right)^{\frac{1}{2}} \quad (11)$$

where S_{pa} (m^2) is the surface area of a single catalyst particle.

Intraparticle distribution method

In the catalyst bed, the mass transfer of reactants first takes place from the bulk fluid to the external surface of catalyst pellets. Then the reactants diffuse into and through pores inside the pellets, with reactions occurring on the pore surface. This two-step diffusion process, including the external and internal diffusion in the porous catalyst pellets, is shown in Fig. 3. Expecting an analogous behavior between the mass diffusion and the heat transfer, the model of the intraparticle heat and mass balances can be developed. A non-isothermal condition is assumed throughout the spherical particle. It is also assumed that the molecular diffusion occurs only in the radial direction within the pellet, and the catalyst particles are spherical or equal to their volume equivalent sphere.

The local reaction rate inside the porous catalyst pellet depends predominately on the local composition and temperature. Hence, the effectiveness factor η_j for reaction j (j = MSR, MD and WGS) is regarded as the ratio of the average rate of reaction j with diffusion inside the catalyst pellet to the rate of reaction in the bulk stream. The average reaction rate can be calculated by the integral of the local reaction rate with respect to the catalyst volume and then divided by the catalyst volume. The effectiveness factor can be approximated by the intraparticle distribution method:

$$\eta_j = \frac{\int_0^{r_p} 4\pi\xi^2 r_j(c_i, T) d\xi}{(4/3)\pi r_p^3 r_j\left(c_i^b, T^b\right)} \quad (12)$$

where ξ (m) is the radial distance of pellet; $r_j(c_i, T)$ (mol m^{-2} s^{-1}) indicates the local rate of reaction j with the temperature T (K) and the concentration c_i (mol m^{-3}) of component i inside the pellet; and $r_j\left(c_i^b, T^b\right)$ (mol m^{-2} s^{-1}) indicates the intrinsic rate of reaction j in the bulk fluid condition with the temperature T^b (K) and the concentration c_i^b (mol m^{-3}) of component i.

The temperature and concentration profiles inside a spherical catalyst particle can be calculated according to the following mass and heat balance equations:

Intraparticle mass balance

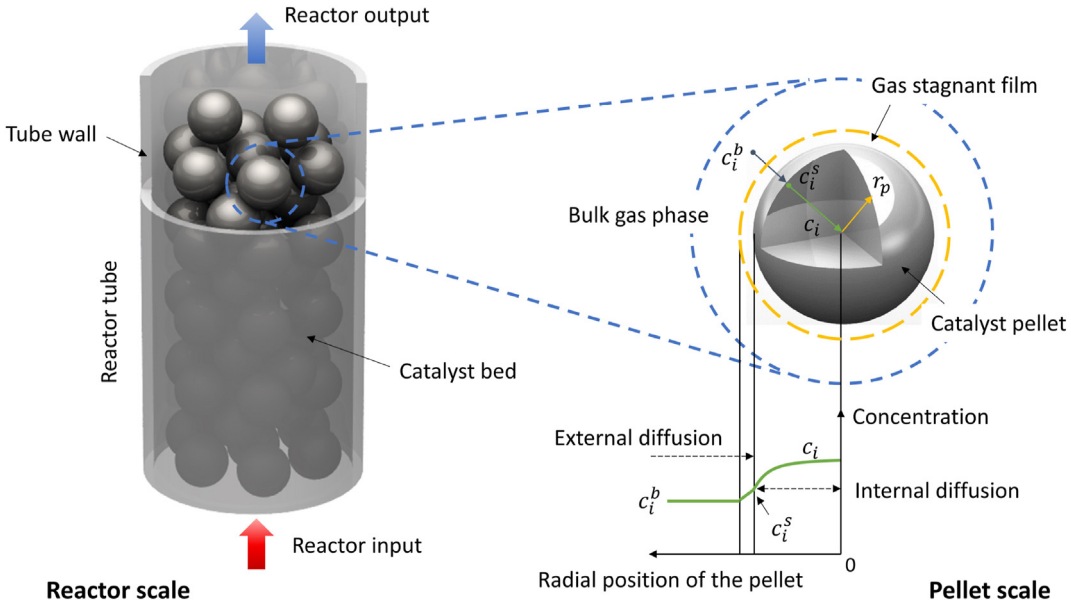

Fig. 3 – Diffusion processes in a catalytic pellet.

Please cite this article as: Zhu J et al., The role of effectiveness factor on the modeling of methanol steam reforming over CuO/ZnO/Al_2O_3 catalyst in a multi-tubular reactor, International Journal of Hydrogen Energy, https://doi.org/10.1016/j.ijhydene.2021.12.223

$$D_{i,ep}\left(\frac{\partial^2 c_i}{\partial \xi^2}+\frac{2}{\xi}\frac{\partial c_i}{\partial \xi}\right)=\rho_c\sum_{j=1}^{N_R}v_{ij}r_jS_c \tag{13}$$

Intraparticle heat balance

$$\lambda_{ep}\left(\frac{\partial^2 T}{\partial \xi^2}+\frac{2}{\xi}\frac{\partial T}{\partial \xi}\right)=\rho_c\sum_{j=1}^{N_R}(-\Delta H_j)r_jS_c \tag{14}$$

where $D_{i,ep}$ ($m^2\,s^{-1}$) is the particle effective diffusivity of component i; λ_{ep} ($W\,m^{-1}\,K^{-1}$) is the particle effective thermal conductivity; v_{ij} is the stoichiometric coefficient of species i in the reaction j; N_R is the number of main reactions; and r_j ($mol\,m^{-2}\,s^{-1}$) is the local rate of reaction j within the catalyst particle.

The boundary conditions are:

at $\xi = 0$,

$$\frac{\partial c_i}{\partial \xi}=0$$

$$\frac{\partial T}{\partial \xi}=0$$

at $\xi = \frac{d_p^v}{2}$,

$$-D_{i,ep}\frac{\partial c_i}{\partial \xi}=k_{i,fs}\left(c_i-c_i^b\right) \tag{15}$$

$$-\lambda_{ep}\frac{\partial T}{\partial \xi}=h_{fs}\left(T-T^b\right) \tag{16}$$

where $k_{i,fs}$ ($m\,s^{-1}$) is the mass transfer coefficient between the bulk fluid and catalyst particle; h_{fs} ($W\,m^{-2}\,K^{-1}$) is the heat transfer coefficient, considering both the external and internal heat transfer, between the bulk fluid and catalyst particle; and d_p^v (m) is the volume-equivalent sphere diameter, which equals the diameter of a sphere with the same volume as the particle.

Species continuity equation

To develop a one-dimensional steady-state model of a multi-tubular packed-bed reactor for the MSR process, the following assumptions are made:

1. the whole system is adiabatic and under steady-state conditions;
2. all reacting species are in the gas phase and behave as the ideal gas;
3. plug flow occurs in a packed bed with no axial mixing;
4. the temperature and concentration gradients in the radial direction are neglected;
5. the catalyst size and packed bed porosity are considered to be uniform.

This model considers the effectiveness factors, pressure drop, heat and mass transfer in tube and shell sides along the reactor length, and heat exchange between the tube side and shell side through the tube wall. The continuity equation for specie i along the axis of the catalyst bed is given by:

$$\frac{dF_i}{dz}=\eta_i r_i \rho_b A_c \tag{17}$$

where F_i ($mol\,s^{-1}$) is the molar flow rate of species i at the axial location z (m), A_c (m^2) is the cross-sectional area of the catalyst bed, r_i ($mol\,kg_{catalyst}^{-1}\,s^{-1}$) is the production rate of component i, $C_{P,i}$ ($J\,mol^{-1}\,K^{-1}$) is the specific heat of gas component i, and ρ_b ($kg\,m^{-3}$) is the density of catalyst bed.

Thermal energy equation

The steady state energy balance along the axis of the catalyst bed leads to the following equation:

$$\frac{dT_t}{dz}=\frac{U_t a\Delta T+\sum r_j\rho_b\Delta H_j S_c}{\sum F_i C_{P,i}}A_c \tag{18}$$

where U_t ($W\,m^{-2}\,K^{-1}$ or $J\,s^{-1}\,m^{-2}\,K^{-1}$) is the overall heat transfer coefficient in tube side, a is the surface-to-volume ratio in the thermal conductivity of a single tube, ΔT (K) is the temperature difference between shell side and tube side, ΔH_j ($J\,mol^{-1}$) is the reaction enthalpy of reaction j, and r_j ($mol\,m^2\,s^{-1}$) is the rate of reaction j.

A steady state energy balance along the axis in shell side is written as:

$$\frac{dT_s}{dz}=\frac{N_s U_s A_o \Delta T}{F_s C_{Ps} L} \tag{19}$$

where U_s ($W\,m^{-2}\,K^{-1}$ or $J\,s^{-1}\,m^{-2}\,K^{-1}$) is the overall heat transfer coefficient outside the tube, A_o (m^2) is the heat transfer area outside the reactor tube, F_s ($mol\,s^{-1}$) is the molar flow rate of burner gas, $C_{P,s}$ ($J\,kg^{-1}\,K^{-1}$) is the specific heat of burner gas, L (m) is the total length of the packed-bed reactor, and N_t is the number of tubes in the reformer.

Pressure drop

It is assumed that a set of porous catalyst pellets of uniform size are packed in the cylindrical tubes. The pressure drop along the reactor length can be approximated by the semi-empirical Ergun equation [21]:

$$\frac{dP}{dz}=-\frac{G}{\rho_f d_p}\left(\frac{1-\varphi}{\varphi^3}\right)\left[\frac{150(1-\varphi)\mu_f}{d_p}+1.75G\right] \tag{21}$$

where μ_f (Pa s) is the viscosity of gas mixture, ρ_f ($kg\,m^{-3}$) is the density of gas mixture, φ is the void fraction of the catalyst bed, and G ($kg\,m^{-2}\,s^{-1}$) is superficial mass velocity. The parameters for modeling in this study are listed in Table 1.

Results and discussion

Model validation

To validate the kinetic model and the effectiveness factor calculated by two different methods (Thiele modules method and intraparticle distribution method) described in section Mathematical model, an experiment was conducted in a

Please cite this article as: Zhu J et al., The role of effectiveness factor on the modeling of methanol steam reforming over CuO/ZnO/Al_2O_3 catalyst in a multi-tubular reactor, International Journal of Hydrogen Energy, https://doi.org/10.1016/j.ijhydene.2021.12.223

Table 1 – Properties of catalyst and geometric parameters of the reactor.

Parameter	Value
Density of catalyst bed, ρ_b (kg m^{-3})	1300
BET area, S_c (m^2 kg^{-1})	102 000
Average pore diameter, Å (m)	6.4×10^{-9}
Void fraction of catalyst bed, φ	0.37
Diameter of cylindrical catalyst particle, d_p (m)	0.001 5
Height of cylindrical catalyst particle, h (m)	0.001 5
Site concentrations of site '1', C^T_{S1} (mol m^{-2})	7.5×10^{-6}
Site concentrations of site '1a', C^T_{S1a} (mol m^{-2})	7.5×10^{-6}
Site concentrations of site '2', C^T_{S2} (mol m^{-2})	7.5×10^{-6}
Site concentrations of site '2a', C^T_{S2a} (mol m^{-2})	7.5×10^{-6}
Number of reactor tubes, N_t	36
Inner diameter of the tubular reactor, D_t (m)	0.016
Outer diameter of the tubular reactor, D_o (m)	0.018
Tube pitch, p_t (m)	0.027
Number of baffle plates, N_b	4
Spacing between baffle plates, p_b (m)	0.12
Length of the reactor, L (m)	0.48
Area fraction of baffle plate that is window, f_b (for 25% baffle plate)	0.195 5

small-scale reactor loaded with porous catalyst particles for MSR reactions. The experimental results were compared with the simulation results of (1) the kinetic model only, (2) the kinetic model + effectiveness factor calculated by the Thiele modules method, and (3) the kinetic model + effectiveness factor calculated by the intraparticle distribution method. Simulation results in terms of the methanol conversion and CO concentration in reformed gas were compared with the experimental data at the operating temperatures of 493 K, 513 K and 533 K, and the W/F_{CH_3OH} ratios of 0–300 kg s mol^{-1}. The operating parameters for simulations and experiments are shown in Table 2.

As shown in Fig. 4, there is a good agreement between the experimental data and the calculated methanol conversions of the model using the intraparticle distribution method, where a percentage discrepancy of less than 3.3% is observed. The kinetic model with effectiveness factors calculated by Thiele modulus also agrees well with the experimental data of methanol conversion, where the maximal percentage discrepancy is 5.4%. Furthermore, for the kinetic model without considering effectiveness factors, a more considerable difference appears between the predicted methanol conversion and the experimental results. Therefore, for cylindrical catalyst particles (1.5 mm diameter with an aspect ratio of 1) used in this study, the effect of catalyst particle size on methanol conversion should be considered owing to the significant effect of intraparticle diffusion on reaction rates.

Fig. 5 shows the comparison between the experimental results and simulated CO concentration in the reformed gas with changes under the operating temperatures and W/F_{CH_3OH}. As we can see, these models can approximately predict the CO concentration under most conditions. However, there are two unexpected jumps of CO concentration in the experimental data when the temperature is at 493 K and 513 K, and the W/F_{CH_3OH} is at 259 kg s mol^{-1}. A possible explanation for this might be the non-uniform distributions of temperature and concentration in the reactor, which affect the local reaction rates. Another possible explanation is that, in our experiments, a very small feeding rate of methanol is introduced to obtain a large W/F_{CH_3OH} in the reactor. This extremely small feeding rate of liquid methanol (0.051 cm^3 min^{-1}) could intensify the effect of non-uniform distributions and lead to the oscillations of CO production at the large W/F_{CH_3OH} value. Moreover, the large void fractions near the reactor wall, which were not investigated in this study, could also be a possible reason.

Intraparticle diffusion

According to the above analysis, the intraparticle distribution method provides a better prediction of effectiveness factors in the catalyst bed. Therefore, this method for the calculation of the effectiveness factors is utilized in this section by solving the mass and heat balance equations governing both the reactions and diffusion inside catalyst pellets. The numerical solutions of the mass and heat balance equations allow the evaluation of both temperature and concentration profiles inside the pellet. Fig. 6 shows the intraparticle profiles of concentration as function of the dimensionless radial position (r/R). To study the intraparticle diffusion phenomena, the concentration profiles are discussed for varying particle diameter $(d_p = 1.0, 2.0\text{mm})$ and varying bulk temperature $(T_b = 493, 553\text{K})$ at the inlet condition $(S/C = 1.3)$ of the catalyst bed. By comparing Fig. 6 (a) with (b), the changes in concentration become more rapid from the external surface $(r/R = 1)$ to the pellet center $(r/R = 0)$ when the diameter increases from 1.0 mm to 2.0 mm. In addition, as the bulk temperature increases from 493 K to 553 K, the changes in concentrations also become more dramatic along the pellet radius. Therefore, the process tends to be more diffusion-limited with increasing particle size and temperature. The methanol conversion is generally reduced due to these diffusion limitations within the catalyst particles. The effect of external mass transfer limitations is also investigated by considering the mass transfer coefficient $k_{i,fs}$ from the gas to solid phase. The mass transfer coefficient is represented as the difference between concentrations on the external catalyst surface and the given values (reactor inlet condition) in the bulk fluid. As shown in Fig. 6, the effect of the external mass transfer resistance is represented as the difference between the concentrations of the diffusing species in the bulk fluid (with 56.5% vol of H_2O and 43.5% vol of CH_3OH) and those on the external surface (when r/R = 1). The results show that there are negligible external mass transfer resistances for this

Table 2 – Geometric and operating parameters for simulations and experiments.

Parameter	Value
Mass of catalyst (g)	3.66
Volume of catalyst bed (mL)	3.6
Feeding rate of methanol liquid (cm^3 min^{-1})	0.051 – 0.308
Operating temperature (K)	493 – 533
Operating pressure (bar)	1
Steam/methanol ratio (S/C) (mol/mol)	1.3
Catalyst size (mm)	1.5 × 1.5
W/F_{CH_3OH} (kg s mol^{-1})	0 – 300

Please cite this article as: Zhu J et al., The role of effectiveness factor on the modeling of methanol steam reforming over CuO/ZnO/Al_2O_3 catalyst in a multi-tubular reactor, International Journal of Hydrogen Energy, https://doi.org/10.1016/j.ijhydene.2021.12.223

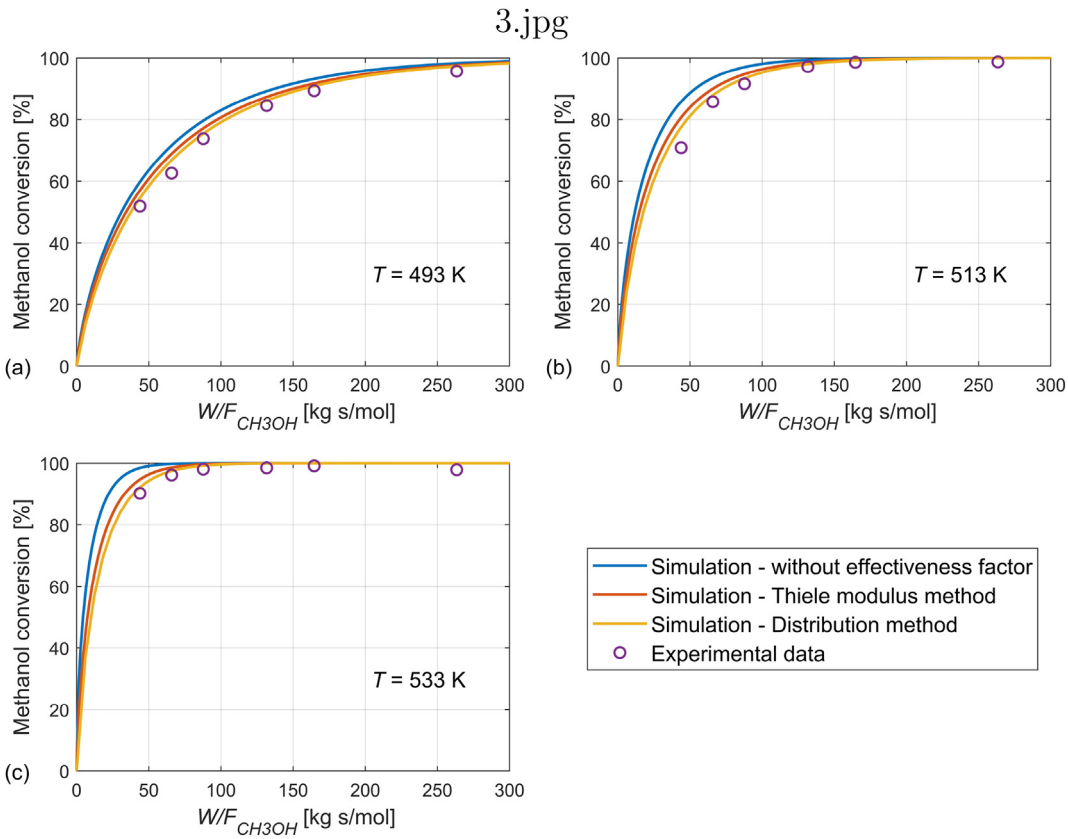

Fig. 4 – Comparison of methanol conversion between the simulation results and the experimental results under different W/F_{CH_3OH} and operating temperatures of catalyst bed.

gas–solids system in these operating conditions, due to the small concentration differences (<1.08%) between the bulk fluid and the external surface. In addition, these concentration differences become slightly larger (from 0.13% to 1.08%) when the bulk fluid temperature is higher and the particle size is larger. Similar results have also been obtained in the study of Hafeez et al. [26] and Zhang et al. [37].

Due to the heat transfer limitations, the effects of particle diameter on the dimensionless profiles of temperature and temperature drop ΔT from the external surface at the inlet condition ($S/C = 1.3$) of the reactor were investigated in this study. With highly endothermic reactions that happen inside porous catalyst particles, heat will be transferred from the bulk fluid through the thermal boundary layer to the external surface of the pellet and then diffuse along the radial direction to the pellet center. Therefore, in Fig. 7(a) and (b), temperatures drop from the external surface to the pellet center due to the heat transfer characteristics and endothermic nature of the MSR process inside the porous catalyst pellet. As the particle diameter increases, temperatures decline more rapidly towards the pellet center due to the greater limitations in internal heat transfer. As can be seen in Fig. 7 (a), there exists a temperature difference between the external surface and the bulk fluid ($T_b = 523K$). This temperature difference increases significantly with the increase in particle size. Therefore, the heat transfer coefficient across the gas-solid interface region due to the external heat transfer limitation can not be neglected. Moreover, the intraparticle distribution of temperature is affected not only by the particle size but also by the bulk fluid temperature. The effects of bulk temperature on the dimensionless profiles of temperature and temperature drop from the external surface (ΔT) are studied. In Fig. 8, the ΔT shows a steeper declining trend from the external surface to the pellet center when a higher temperature of bulk fluid is introduced in the reactor. The reason could be that the increased temperature of the catalyst pellet enhances reaction rates.

Since the effectiveness factor is derived from the intraparticle profiles of concentrations and temperature, the changes in particle size and bulk temperature will also affect the effectiveness factor for each reaction. In Fig. 9, the effects of changes in particle diameter and bulk temperature on the effectiveness factors for MSR and MD reactions are presented at the reactor inlet condition ($S/C = 1.3$). As shown in Fig. 9 (a), when the diameter of catalyst particle approaches zero, the effect of intraparticle diffusion resistances is reduced to the minimum, which is illustrated by the effectiveness factors approaching unity. At this point, the exposure of the catalyst surface to reactants is maximized for the reactions to take place. As the particle diameter increases to 3.0 mm, there will be considerable increases in the heat and mass transfer limitations within the pellet. Hence, the effectiveness factor for the MSR reaction decreases to 0.17, and the effectiveness factor for the MD reaction decreases to 0.036. This implies that

Please cite this article as: Zhu J et al., The role of effectiveness factor on the modeling of methanol steam reforming over CuO/ZnO/Al_2O_3 catalyst in a multi-tubular reactor, International Journal of Hydrogen Energy, https://doi.org/10.1016/j.ijhydene.2021.12.223

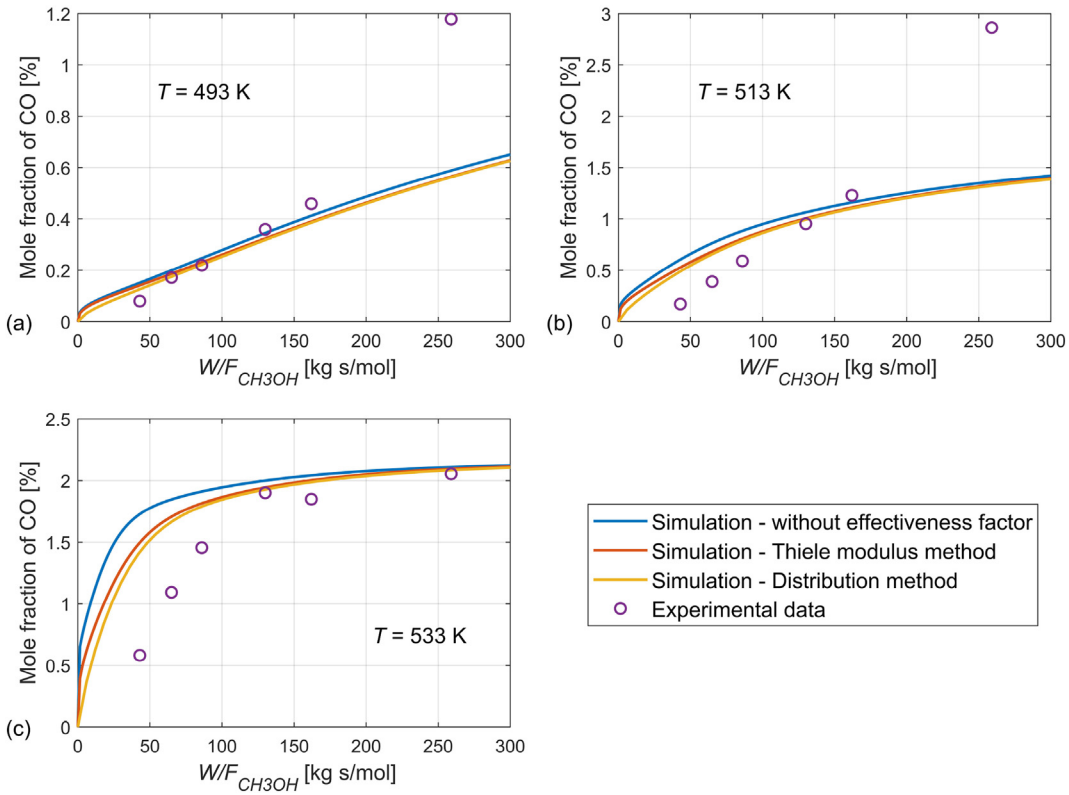

Fig. 5 – Comparison of the mole fraction of CO in the reformed gas between the simulation results and the experimental results under different W/F_{CH_3OH} and operating temperatures of catalyst bed.

for a larger particle diameter, the effect of intraparticle diffusion limitations becomes more predominant. Hence, less surface area in the catalyst is available for the reactions, and, on the contrary, most of the reactions occur near the external surface of the catalyst particle. As shown in Fig. 9(b), when the bulk fluid temperature increases from 273 K to 573 K, the effectiveness factor for the MSR reaction decreases from almost 1 to 0.1, and the effectiveness factor for the MD reaction decreases from 0.96 to 0.03. For a very high temperature in the bulk fluid, the reaction rate is enhanced and becomes more significant than the diffusion rate. Thus the effectiveness factors become smaller, and the process is regarded as diffusion-limited. Most of the reactants are consumed very fast near the outer surface when diffusing towards the pellet center. Therefore, only a very small amount of reactants can penetrate the interior of the pellet.

Reformer performance

By developing the one-dimensional pseudo-homogeneous model, the performance of the MSR process on a multi-tubular packed-bed reformer is predicted. The MSR process in this reformer operates under the given conditions that the W/F_{CH_3OH} is 235 kg s mol^{-1}, the inlet temperature of shell-side gas is 673 K, and the inlet temperature of water-methanol vapor mixture is 473 K. In Fig. 10, the solid lines show the simulation results with effectiveness factors calculated by the intraparticle distribution method and the' + ' plus signs refer to the simulation results with effectiveness factors using the Thiele modulus method. There are only slight differences between the profiles by these two methods, which indicates that both the intraparticle distribution method and the Thiele modulus method can be used to predict the effectiveness factors for the MSR process in this reactor. Other results comparisons between these two methods under different temperatures of the burner gas and different particle sizes can be found in the Appendix. The concentration profiles of reactants and products along the reactor length are displayed in Fig. 10 (a). As can be seen, the methanol-steam mixture is fed into the reactor with an S/C of 1.3. As the reaction proceeds, the mole fractions of reforming products constantly increase along the reactor length. After reactants pass through the catalyst bed, a methanol conversion of 98% is obtained. However, about 90% of the methanol is converted by the MSR process in the front section of the tube, which can be seen in Fig. 10 (c). Fig. 10 (b) shows a transient rise of temperature in the catalyst bed and a transient decrease of temperature in the burner gas near the tube entrance. This is due to the considerable temperature difference between the shell and tube sides, enhancing the heat transfer. Fig. 10 (d) shows the profiles of effectiveness factors for MSR, MD and WGS reactions under the same operating conditions. The change of the effectiveness factor for the MSR reaction represents a similar trend with that for the MD reaction, while it shows a

Please cite this article as: Zhu J et al., The role of effectiveness factor on the modeling of methanol steam reforming over CuO/ZnO/Al_2O_3 catalyst in a multi-tubular reactor, International Journal of Hydrogen Energy, https://doi.org/10.1016/j.ijhydene.2021.12.223

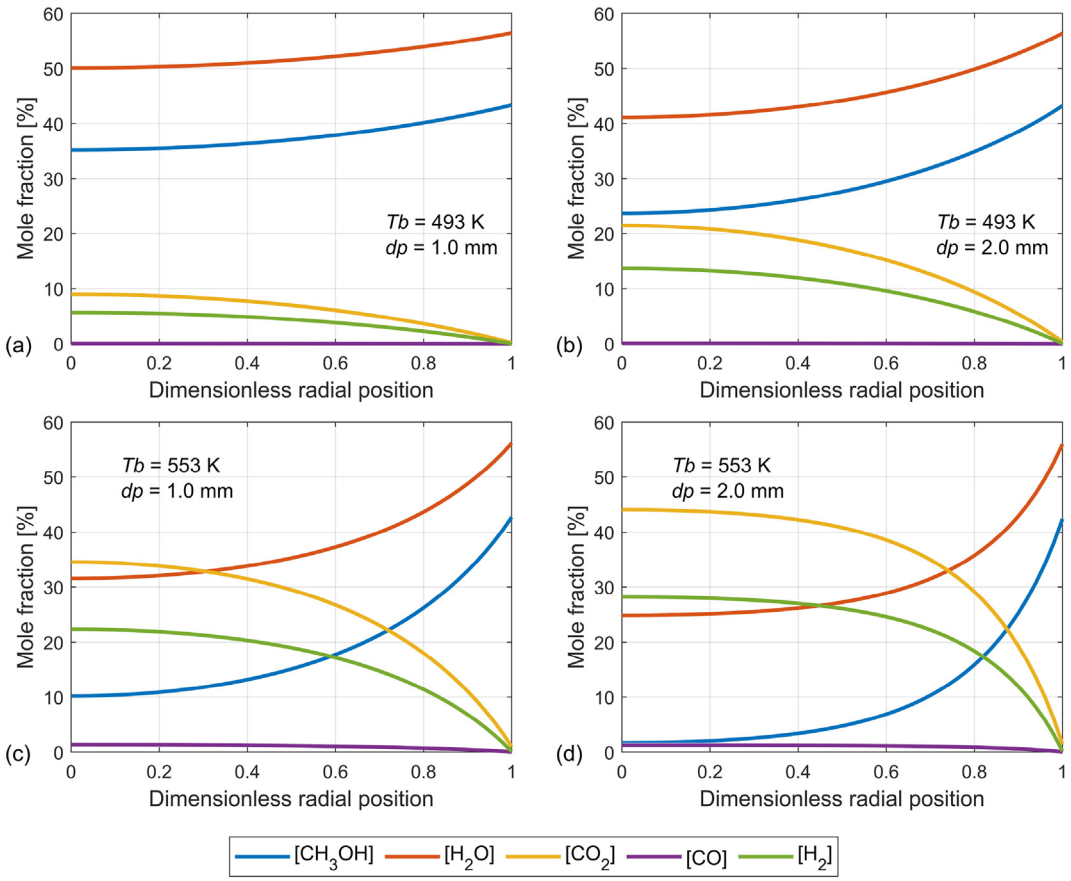

Fig. 6 – Simulated intraparticle profiles of mole fractions from the pellet center to the external radius of the pellet at the inlet condition for varying temperature T_b and diameter of catalyst particle d_p: (a) $T_b = 493$ K, $d_p = 1.0$ mm; (b) $T_b = 493$ K, $d_p = 2.0$ mm; (c) $T_b = 553$ K, $d_p = 1.0$ mm; and (d) $T_b = 553$ K, $d_p = 2.0$ mm.

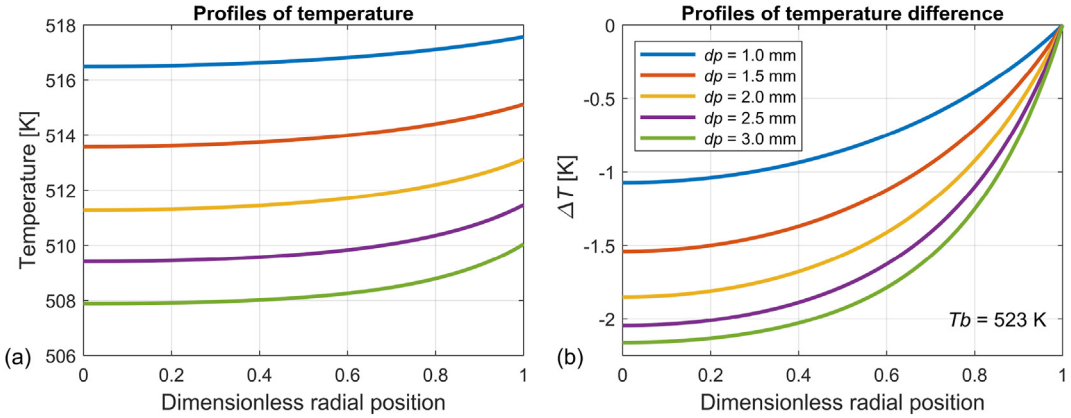

Fig. 7 – Intraparticle profiles of (a) temperature and (b) temperature difference from the pellet center to the external radius of the pellet at the inlet condition for varying diameter of catalyst particle d_p.

hyperbolic trend along the reactor for the WGS reaction. This could be due to the fact that the WGS reaction is reversed along the reactors.

Due to the effect on the intraparticle diffusion limitations, the change in particle diameter d_p is observed to have effects on the profiles of the methanol conversion and pressure drop through the length of the catalyst bed, which is presented in Fig. 11. The inlet temperature of burner gas in the shell side T_s is 673 K, the inlet temperature of water/methanol vapor T_t is 433 K, and the W/F_{CH_3OH} is 235 kg s mol^{-1} in this reactor. In Fig. 11 (a), it is found that the methanol conversion is slightly increased from 94.92% to 97.16% when the diameter of the catalyst particle decreases from 2.5 mm to 0.5 mm. This is caused by the decrease of intraparticle diffusion resistances.

Please cite this article as: Zhu J et al., The role of effectiveness factor on the modeling of methanol steam reforming over CuO/ZnO/Al_2O_3 catalyst in a multi-tubular reactor, International Journal of Hydrogen Energy, https://doi.org/10.1016/j.ijhydene.2021.12.223

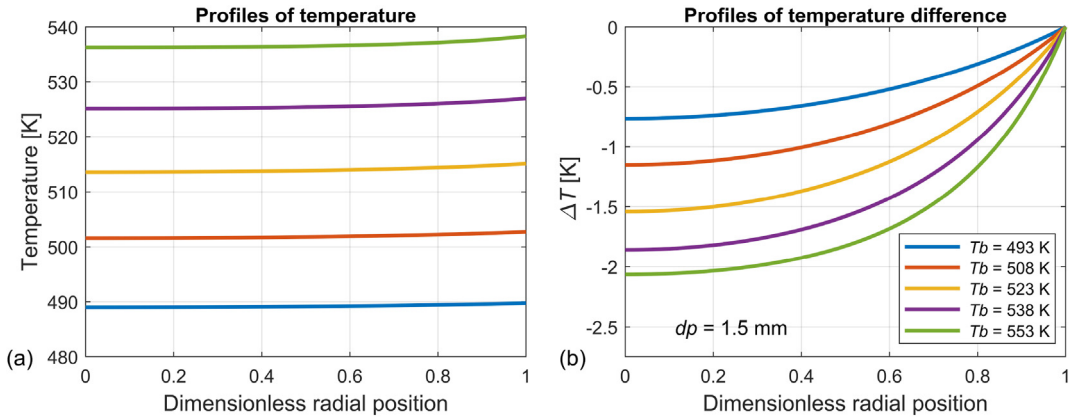

Fig. 8 – Intraparticle profiles of (a) temperature and (b) temperature difference from the pellet center to the external radius of the pellet at the inlet condition for varying bulk fluid temperature T_b.

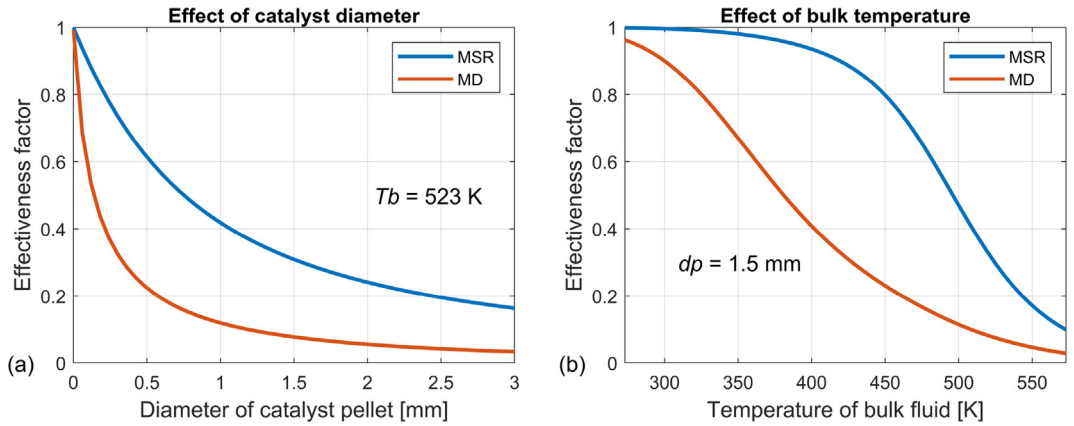

Fig. 9 – Effects of (a) catalyst diameter d_p and (b) bulk fluid temperature T_b variations on effectiveness factors for MSR and MDreactions at the reactor inlet condition.

However, as shown in Fig. 11 (b), a remarkable increase of pressure drop along the reactor length is observed when using a smaller particle size. Excessive pressure drop or pressure loss in the reactor tubes should generally be avoided, because it will result in poor system performance and excessive pump power consumption. A catalyst particle diameter of less than 1.5 mm is acceptable for the reaction process as it is still within the allowed 10% (difference from the initial pressure) pressure drop for the packed-bed reactor [24].

Optimization of operating parameters

As additional heat is provided from the burner gas in the shell side as the reactants flow through the catalyst bed, the inlet temperature of burner gas can affect the methanol conversion and CO concentration by affecting the heat transfer through the tube wall. In Fig. 12 (b), the methanol conversion is improved when increasing the inlet temperature of burner gas from 573 K to 773 K because more heat is provided to the catalyst bed. However, as shown in Fig. 12 (a), there is also a dramatic increase of CO concentration in the reformed gas due to the increased temperature of burner gas. The increase in temperature favors endothermic reactions (MD and reverse WGS), which leads to the accelerated CO production rate. Fig. 12(a) and (b) also illustrate the changes in methanol conversion and CO concentration with the W/F_{CH_3OH} ranging from 100 to 350 kg s mol^{-1}, where the inlet flow of methanol is changed at constant catalyst loading. The methanol conversion is increased by increasing the W/F_{CH_3OH}, so does the CO concentration in the reformed gas. This is because less methanol is fed into the catalyst bed to gain a larger value of W/F_{CH_3OH}, which leads to the reduction in the energy consumption by the MSR reforming process. Therefore, the increased temperature in the catalyst bed enhances the selectivity of CO.

Many studies have been conducted on the poisoning effects of methanol-based reformate impurities on the PBI-based HT-PEM fuel cells. Generally, a CO concentration of 2–3% vol and a methanol concentration of 3% vol in the anode stream can be tolerated without leading to a significant degradation in the performance of the HT-PEM fuel cell [38–40]. However, the poisoning effects can deteriorate due to the possible interdependence among the effects of different impurities and can have more long-term severe durability effects on the fuel cell [39]. Therefore, keeping the concentrations of CO and methanol to less than 1% vol in the reformate gas is expected to be a good compromise and is used to optimize the operating parameters of the MSR process in the

Please cite this article as: Zhu J et al., The role of effectiveness factor on the modeling of methanol steam reforming over CuO/ZnO/Al_2O_3 catalyst in a multi-tubular reactor, International Journal of Hydrogen Energy, https://doi.org/10.1016/j.ijhydene.2021.12.223

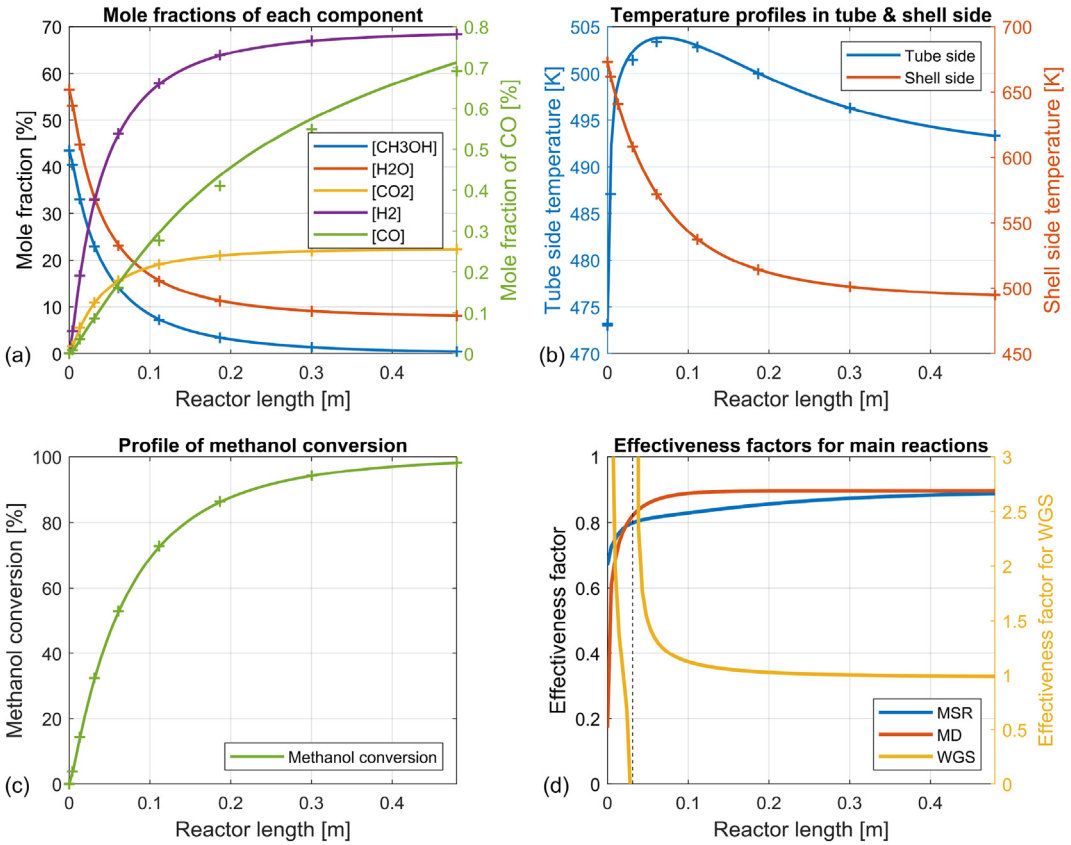

Fig. 10 – Profiles of (a) mole fractions of each component, (b) temperature in both tube and shell sides, (c) methanol conversion and (d) effectiveness factors for MSR, MD and WGS reactions along the reactor length with effectiveness factors calculated by the intraparticle distribution method (solid line) and Thiele modulus method ('+' plus sign).

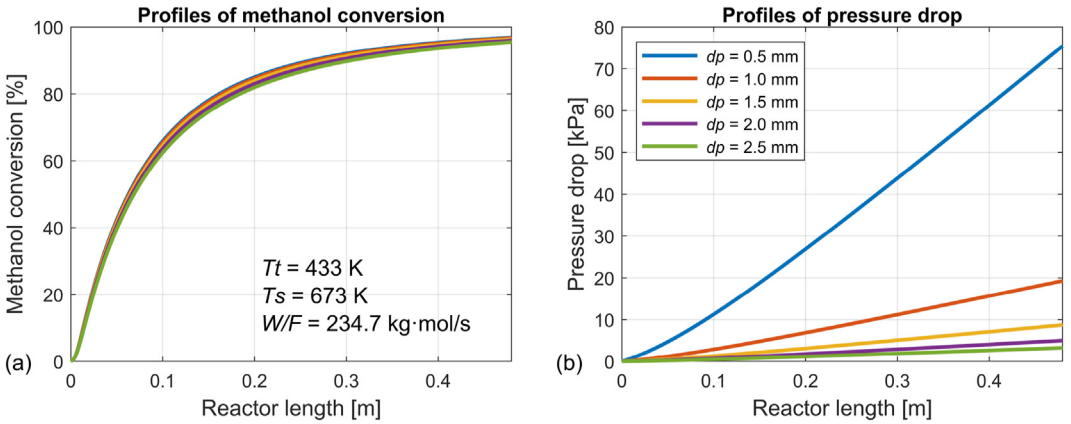

Fig. 11 – Effects of the diameter of catalyst particles d_p on distributions of (a) the methanol conversion, and (b) the pressure drop along the reactor length.

reformer. In Fig. 12(a) and (b), the 1% vol line of CO and methanol concentration is highlighted in each profile, which corresponds to *L*1 and *L*2 in Fig. 12 (c), respectively. In Fig. 12 (c), the area on the left side of *L*1 corresponds to CO concentration lower than 1% vol, and the area on the right side of *L*2 corresponds to methanol concentration lower than 1% vol. Therefore, the operating conditions in area *A* between *L*1 and *L*2 bring both methanol and CO concentration lower than 1% vol, which fulfill the requirement of HT-PEM fuel cells. For example, with the W/F_{CH_3OH} at 300 kg s mol^{-1}, the recommended inlet temperature of burner gas should be in the range of 624–661 K; and with the inlet temperature of burner gas at 773 K, the recommended values of W/F_{CH_3OH} are in the range of 156–174 kg s mol^{-1}.

Please cite this article as: Zhu J et al., The role of effectiveness factor on the modeling of methanol steam reforming over CuO/ZnO/Al_2O_3 catalyst in a multi-tubular reactor, International Journal of Hydrogen Energy, https://doi.org/10.1016/j.ijhydene.2021.12.223

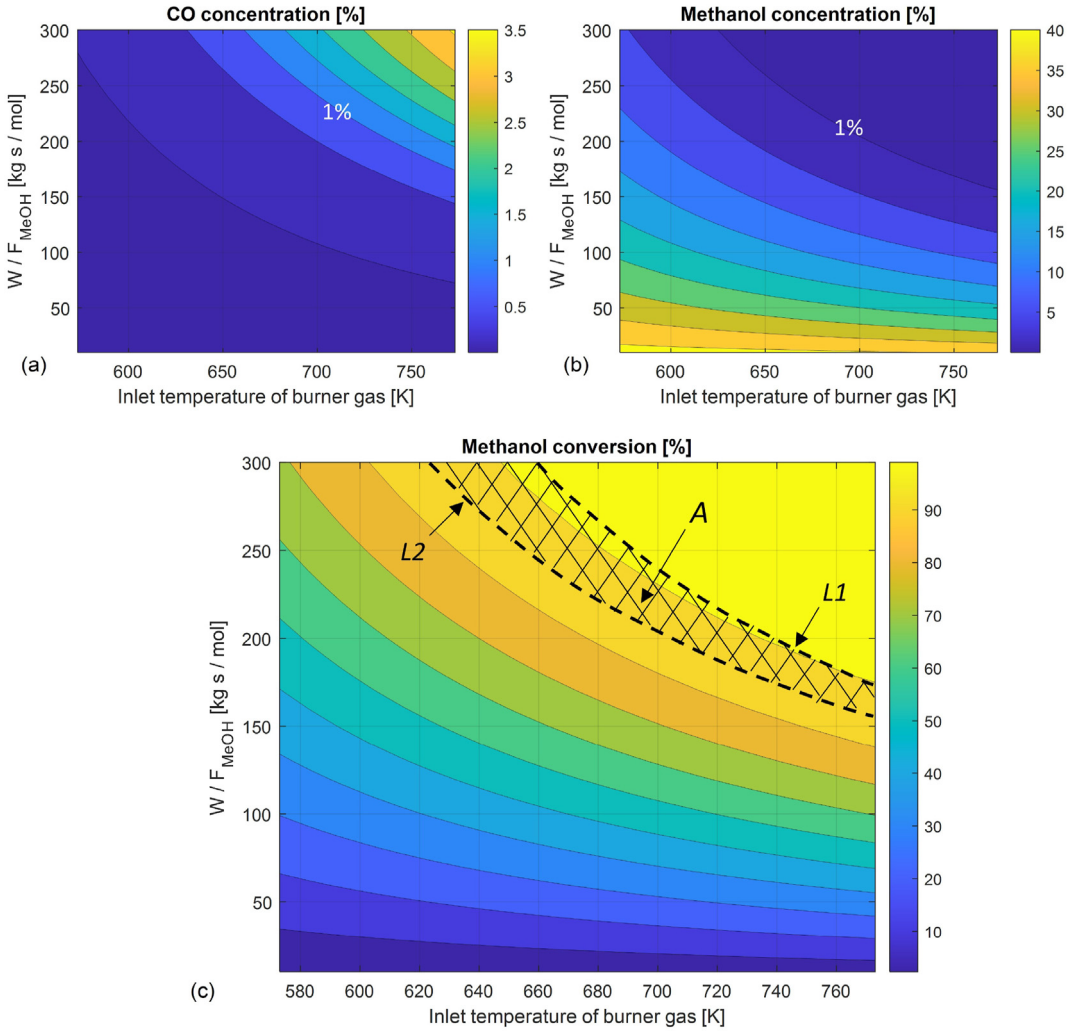

Fig. 12 – Effects of the W/F_{CH_3OH} and the inlet temperature of the burner gas on profiles of (a) the CO concentration, (b) the methanol concentration and (c) methanol conversion in the reformate gas.

Conclusions

A one-dimensional steady-state model of a multi-tubular packed-bed reactor was developed for the MSR on a commercial $CuO/ZnO/Al_2O_3$ catalyst. This model took into account the reaction kinetics, pressure drop, internal and external diffusion resistances of catalyst pellets, heat and mass transfer in both tube and shell sides, and heat exchange between the tube and shell sides through the tube wall. To predict the effectiveness factors for main reactions, both the intraparticle distribution method and the Thiele modulus method were adopted and compared in this work. The computational results of both methods showed good agreements with the experimental results for methanol conversion and CO concentration, but the intraparticle distribution method provided better predictions. Therefore, the effect of the particle size on the one-dimensional profiles of methanol conversion and CO concentration were investigated by the intraparticle distribution method. The results indicated that the methanol conversion was improved with the decrease in particle size, which also brings a higher pressure drop over the catalyst bed. Moreover, the effects of the inlet temperature of burner gas and W/F_{CH_3OH} on methanol conversion and CO concentration in the reformate gas were analyzed. It was observed that the increase in the inlet temperature of burner gas and the increase in W/F_{CH_3OH} could improve the methanol conversion, but also lead to a higher CO concentration in the products. Based on the computational results, the optimized operation conditions that bring both methanol and CO concentration lower than 1% vol in products were determined. With the W/F_{CH_3OH} at 300 kg s mol^{-1}, the recommended inlet temperature of burner gas should be in the range of 624–661 K; and with the inlet temperature of burner gas at 773 K, the recommended values of W/F_{CH_3OH} are in the range of 156–174 kg s mol^{-1}.

Declaration of competing interest

The authors declare that they have no known competing financial interests or personal relationships that could have appeared to influence the work reported in this paper.

Please cite this article as: Zhu J et al., The role of effectiveness factor on the modeling of methanol steam reforming over $CuO/ZnO/Al_2O_3$ catalyst in a multi-tubular reactor, International Journal of Hydrogen Energy, https://doi.org/10.1016/j.ijhydene.2021.12.223

Acknowledgements

The research leading to these results has received funding from the Chinese scholarship council (CSC) and from the Danish Energy Technology Development and Demonstration Program (EUDP) through the COmmercial BReakthrough of Advanced fuel cells (COBRA Drive) project, grant number 64018-0118.

Appendix A. Supplementary data

Supplementary data to this article can be found online at https://doi.org/10.1016/j.ijhydene.2021.12.223.

REFERENCES

[1] Lan H, Yang L, Zheng F, Zong C, Wu S, Song X. Analysis and optimization of high temperature proton exchange membrane (ht-pem) fuel cell based on surrogate model. Int J Hydrogen Energy 2020;45(22):12501–13.
[2] Bodner M, García HR, Steenberg T, Terkelsen C, Alfaro SM, Avcioglu GS, Vassiliev A, Primdahl S, Hjuler HA. Enabling industrial production of electrodes by use of slot-die coating for ht-pem fuel cells. Int J Hydrogen Energy 2019;44(25):12793–801.
[3] Xia L, Zhang C, Hu M, Jiang S, Chin CS, Gao Z, Liao Q. Investigation of parameter effects on the performance of high-temperature pem fuel cell. Int J Hydrogen Energy 2018;43(52):23441–9.
[4] Özcan O, Akın AN. Thermodynamic analysis of methanol steam reforming to produce hydrogen for HT-PEMFC: an optimization study. Int J Hydrogen Energy 2019;44(27):14117–26. https://doi.org/10.1016/j.ijhydene.2018.12.211.
[5] Das SK, Reis A, Berry KJ. Experimental evaluation of CO poisoning on the performance of a high temperature proton exchange membrane fuel cell. J Power Sources 2009;193(2):691–8. https://doi.org/10.1016/j.jpowsour.2009.04.021.
[6] Abe JO, Popoola A, Ajenifuja E, Popoola O. Hydrogen energy, economy and storage: review and recommendation. Int J Hydrogen Energy 2019;44(29):15072–86.
[7] Dawood F, Anda M, Shafiullah G. Hydrogen production for energy: an overview. Int J Hydrogen Energy 2020;45(7):3847–69.
[8] Chougule A, Sonde RR. Modelling and experimental investigation of compact packed bed design of methanol steam reformer. Int J Hydrogen Energy 2019;44(57):29937–45. https://doi.org/10.1016/j.ijhydene.2019.09.166.
[9] Léonard G, Giulini D, Villarreal-Singer D. Design and evaluation of a high-density energy storage route with CO2 re-use, water electrolysis and methanol synthesis. Comput Aided Chem Eng 2016;38:1797–802.
[10] Simon Araya S, Liso V, Cui X, Li N, Zhu J, Sahlin SL, Jensen SH, Nielsen MP, Kær SK. A review of the methanol economy: the fuel cell route. Energies 2020;13(3):596.
[11] Yong ST, Ooi CW, Chai SP, Wu XS. Review of methanol reforming-Cu-based catalysts, surface reaction mechanisms, and reaction schemes. Int J Hydrogen Energy 2013;38(22):9541–52. https://doi.org/10.1016/j.ijhydene.2013.03.023.
[12] Chen WH, Su YQ, Lin BJ, Kuo JK, Kuo PC. Hydrogen production from partial oxidation and autothermal reforming of methanol from a cold start in sprays. Fuel 2021;287:1–9.
[13] Peppley BA, Amphlett JC, Kearns LM, Mann RF. Methanol–steam reforming on Cu/ZnO/Al2O3. Part 1: the reaction network. Appl Catal Gen 1999;179(1–2):21–9. https://doi.org/10.1016/s0926-860x(98)00298-1.
[14] Peppley BA, Amphlett JC, Kearns LM, Mann RF. Methanol–steam reforming on Cu/ZnO/Al2O3 catalysts. Part 2. A comprehensive kinetic model. Appl Catal Gen 1999;179(1–2):31–49. https://doi.org/10.1016/s0926-860x(98)00299-3.
[15] Palo DR, Dagle RA, Holladay JD. Methanol steam reforming for hydrogen production. Chem Rev 2007;107(10):3992–4021.
[16] Azenha C, Lagarteira T, Mateos-Pedrero C, Mendes A. Production of hydrogen from methanol steam reforming using cupd/zro2 catalysts–influence of the catalytic surface on methanol conversion and co selectivity. Int J Hydrogen Energy 2021;46(33):17490–9.
[17] Agarwal V, Patel S, Pant KK. H2 production by steam reforming of methanol over Cu/ZnO/Al2O3 catalysts: transient deactivation kinetics modeling. Appl Catal Gen 2005;279(1–2):155–64. https://doi.org/10.1016/j.apcata.2004.10.026.
[18] Méndez CI, Ancheyta J, Trejo F. Modeling of catalytic fixed-bed reactors for fuels production by Fischer–Tropsch synthesis. Energy Fuels 2017;31(12):13011–42. https://doi.org/10.1021/acs.energyfuels.7b01431.
[19] Purnama H, Ressler T, Jentoft RE, Soerijanto H, Schlögl R, Schomäcker R. CO formation/selectivity for steam reforming of methanol with a commercial CuO/ZnO/Al2O3 catalyst. Appl Catal Gen 2004;259(1):83–94. https://doi.org/10.1016/j.apcata.2003.09.013.
[20] Cruz BM, Silva JDD. A two-dimensional mathematical model for the catalytic steam reforming of methane in both conventional fixed-bed and fixed-bed membrane reactors for the Production of hydrogen. Int J Hydrogen Energy 2017;42:23670–90.
[21] Fogler HS. Essentials of chemical reaction engineering: essenti chemica reactio engi. Pearson Education; 2010.
[22] Pathak S, Goswami A, Upadhyayula S. Kinetic modeling and simulation of catalyst pellet in the high temperature sulfuric acid decomposition section of iodine-sulfur process. Int J Hydrogen Energy 2019;44(59):30850–64.
[23] Saeidi S, Najari S, Gróf G, Gallucci F. Effect of operating conditions and effectiveness factor on hydrogenation of co2 to hydrocarbons. Int J Hydrogen Energy 2019;44(54):28586–602.
[24] Iordanidis AA. Mathematical modeling of catalytic fixed bed reactors. The Netherlands: Twente University Press Enschede; 2002.
[25] Lattanzi AM, Pecha MB, Bharadwaj VS, Ciesielski PN. Beyond the effectiveness factor: multi-step reactions with intraparticle diffusion limitations. Chem Eng J 2020;380:122507.
[26] Hafeez S, Aristodemou E, Manos G, Al-Salem SM, Constantinou A. Modelling of packed bed and coated wall microreactors for methanol steam reforming for hydrogen production. RSC Adv 2020;10(68):41680–92. https://doi.org/10.1039/d0ra06834a.
[27] Cui X, Kær SK. A comparative study on three reactor types for methanol synthesis from syngas and CO2. Chem Eng J 2020;393. https://doi.org/10.1016/j.cej.2020.124632. 124632–124632.
[28] Ziarati M, Roozbahani MAG, Khandan N. New method of rigorous modeling and CFD simulation for methanol—steam

reforming in packed-bed reactors. Chem Eng Commun 2016;203(10):1359–73. https://doi.org/10.1080/00986445.2016.1198333.
[29] Olatunde AO, Olafadehan OA, Usman MA. Computation of effectiveness factor for methanol steam reforming over Cu/ZnO/Al2O3 catalyst pellet. Appl Petrochem Res 2020;10(1):35–47. https://doi.org/10.1007/s13203-020-00244-w.
[30] Tesser R, Serio MD, Santacesaria E. Methanol steam reforming: a comparison of different kinetics in the simulation of a packed bed reactor. Chem Eng J 2009;154(1–3):69–75. https://doi.org/10.1016/j.cej.2009.06.007.
[31] Zhu J, Araya SS, Cui X, Sahlin SL, Kær SK. Modeling and design of a multi-tubular packed-bed reactor for methanol steam reforming over a Cu/ZnO/Al2O3 catalyst. Energies 2020;13(3). https://doi.org/10.3390/en13030610. 610–610.
[32] Zhuang X, Xia X, Xu X, Li L. Experimental investigation on hydrogen production by methanol steam reforming in a novel multichannel micro packed bed reformer. Int J Hydrogen Energy 2020;45:11024–58.
[33] Sá S, Sousa JM, Mendes A. Steam reforming of methanol over a CuO/ZnO/Al2O3 catalyst, part I: kinetic modelling. Chem Eng Sci 2011;66(20):4913–21. https://doi.org/10.1016/j.ces.2011.06.063.
[34] Herdem MS, Mundhwa M, Farhad S, Hamdullahpur F. Multiphysics modeling and heat distribution study in a catalytic microchannel methanol steam reformer. Energy Fuels 2018;32(6):7220–34. https://doi.org/10.1021/acs.energyfuels.8b01280.
[35] Peppley BAD. A comprehensive kinetic model of methanol-steam reforming on cu/zno/al o catalyst. Royal Military College of Canada; 1998. Ph.D. thesis.
[36] Driessen RT, Kersten SR, Brilman DW. A Thiele modulus approach for nonequilibrium adsorption processes and its application to CO2 capture. Ind Eng Chem Res 2020;59(15):6874–85. https://doi.org/10.1021/acs.iecr.9b05503.
[37] Zhang G, Zhao J, Wang Q, Yang T, Zhang Q, Zhang L. Fast start-up structured cufemg/al2o3 catalyst applied in microreactor for efficient hydrogen production in methanol steam reforming. Chem Eng J 2021:130644.
[38] Zhou F, Andreasen SJ, Kær SK, Park JO. Experimental investigation of carbon monoxide poisoning effect on a PBI/H3PO4 high temperature polymer electrolyte membrane fuel cell: influence of anode humidification and carbon dioxide. Int J Hydrogen Energy 2015;40(43):14932–41. https://doi.org/10.1016/j.ijhydene.2015.09.056.
[39] Araya S, Andreasen S, Kær S. Experimental characterization of the poisoning effects of methanol-based reformate impurities on a PBI-based high temperature PEM fuel cell. Energies 2012;5(11):4251–67. https://doi.org/10.3390/en5114251.
[40] Araya SS, Grigoras IF, Zhou F, Andreasen SJ, Kær SK. Performance and endurance of a high temperature PEM fuel cell operated on methanol reformate. Int J Hydrogen Energy 2014;39(32):18343–50. https://doi.org/10.1016/j.ijhydene.2014.09.007.

Please cite this article as: Zhu J et al., The role of effectiveness factor on the modeling of methanol steam reforming over CuO/ZnO/Al_2O_3 catalyst in a multi-tubular reactor, International Journal of Hydrogen Energy, https://doi.org/10.1016/j.ijhydene.2021.12.223